Multiscale analysis of the space-time properties in incompressible wall-bounded turbulence

Tian Liang,[1] Cheng Cheng,[1,2] and Lin Fu[1,3,4,5,*]

[1]*Department of Mechanical and Aerospace Engineering, The Hong Kong University of Science and Technology, Clear Water Bay, Kowloon, Hong Kong*

[2]*Institute for Advanced Study, The Hong Kong University of Science and Technology, Clear Water Bay, Kowloon, Hong Kong*

[3]*Department of Mathematics, The Hong Kong University of Science and Technology, Clear Water Bay, Kowloon, Hong Kong*

[4]*HKUST Shenzhen–Hong Kong Collaborative Innovation Research Institute, Futian, Shenzhen, China*

[5]*Center for Ocean Research in Hong Kong and Macau, The Hong Kong University of Science and Technology, Clear Water Bay, Kowloon, Hong Kong*

(Received 4 December 2023; accepted 5 April 2024; published 10 May 2024)

It is believed that the space-time correlation is a fundamental statistical tool for analyzing the dynamic coupling between spatial and temporal scales of the motion in turbulent flows. In this paper, by coupling the inner-outer interaction model with the attached-eddy hypothesis, the space-time correlations of both wall-shear fluctuations and the streamwise velocity fluctuations carried by wall-attached eddies at a given length scale are investigated. The present results demonstrate that the space-time correlations for the wall-shear stress fluctuation are mainly dominated by near-wall small-scale motions and the superposition effects generated by wall-attached eddies are only reflected in the weakly correlated regions with large space separations and/or time delays. Furthermore, the findings in the present study demonstrate that wall-attached eddies at a given length scale feature distinctly different space-time properties as compared to those of ensembled eddies with multiple length scales, which provides an alternative perspective for analyzing the decorrelation mechanisms in turbulence theory and developing an advanced space-time correlation model.

DOI: 10.1103/PhysRevFluids.9.054606

I. INTRODUCTION

A fundamental concept in the statistical theory of turbulence is that the energy-containing eddy is progressively decorrelated in time. The corresponding decorrelation process can be characterized by the correlation of fluctuating velocities at two different points in space and time, known as the space-time correlation. The space-time correlation is widely applicable to turbulence research from both fundamental and practical viewpoints. From a fundamental perspective, it quantifies how turbulent fluctuations at one location and a specific time covary with those at another location and time instant and thus is crucial for understanding the physical mechanisms of spatially developed boundary-layer flow structures [1] as well as their time evolution [2]. From a practical perspective, a space-time-correlation model describes the dynamic behaviors of turbulent fluctuations across both spatial and temporal scales [3] and is beneficial for the development of time-accurate turbulence models for large-eddy simulations [4–8] as well as advanced prediction methodologies for aeroacoustics [9].

*Corresponding author: linfu@ust.hk

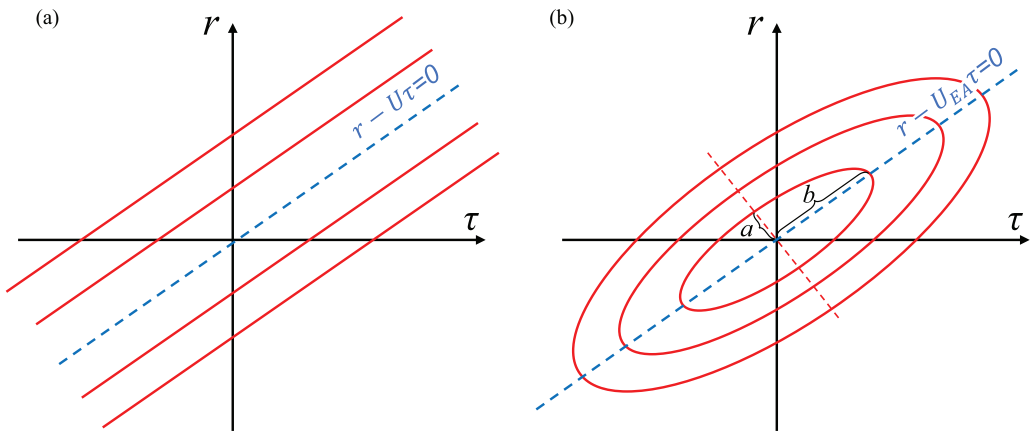

FIG. 1. Schematic diagrams for the isocorrelation contours: (a) straight lines with a constant slope in Taylor's frozen-flow hypothesis and (b) elliptic curves with a uniform preference direction and a constant aspect ratio in the EA model.

The first model to describe space-time correlations in turbulence is known as Taylor's frozen-flow hypothesis [10], which suggests that the spatial patterns of turbulent motion can be transported past a fixed location entirely by the mean flow, and the corresponding advection speed is generally taken as the local average streamwise flow velocity (referred to as the speed of the wind stream in Taylor's original paper). As a result, the relation connecting the velocity signals between two locations with temporal separation τ can be derived as

$$u(x+r, t+\tau) = u(x+r-U\tau, t), \tag{1}$$

where x and r denote the spatial flow coordinate and the spatial separation, respectively, t and τ denote the physical time and temporal separation, respectively, and U denotes the local average streamwise flow velocity. Consequently, the corresponding space-time correlation can be defined as

$$R(r, \tau) = \langle u(x, t)u(x+r, t+\tau)\rangle = R(r-U\tau, 0), \tag{2}$$

where $\langle\cdot\rangle$ represents the averaging in the temporal and spatially homogeneous directions. This model has been widely utilized to evaluate the spatial energy spectrum in hot-wire measurements [11] and reconstruct space-time energy spectra in particle image velocimetry measurements [12]. Furthermore, Taylor's hypothesis generates new insights into the spatiotemporal dynamics of turbulence, such as the dominant convection process [13] and the propagation velocity of turbulence structures [14]. With Taylor's hypothesis, the space-time correlation can be purely described by the space correlation through a linear transformation $r - U\tau$. However, it is easily understood that Taylor's hypothesis intuitively has some limitations [15], such as the weak shear rate and low turbulence intensity, since the frozen-flow assumption implies that the space-time correlation remains a constant (not decaying) for any given spatial separation r and temporal separation τ along the characteristic line $r - U\tau = C$, where C depends on the contour level [as shown in Fig. 1(a)].

He and Zhang proposed the elliptic approximation (EA) model for turbulent shear flows [16]. The EA model specifies that the small-scale turbulent motion is convected by mean flows while being distorted by the shearing of mean flows and the sweeping of energy-containing eddies in fluctuating velocity fields. Correspondingly, the space-time correlation in shear flows can be described by the space correlation through a transformation

$$R(r, \tau) = R[\sqrt{(r-U\tau)^2 + V^2\tau^2}, 0], \tag{3}$$

where U indicates the local convection velocity of the turbulence flow patterns and the sweeping characteristic velocity V denotes the sum of the random sweeping velocity manifesting the turbulence intensity and the shear-induced velocity, which takes into account the shear effects explicitly up to the second-order time derivatives of fluctuating velocities [17]. Compared with Taylor's classical frozen-flow model, which determines the decorrelation only by the convection velocity, the EA model not only manifests the convection effect but also integrates Kraichnan's sweeping hypothesis [18], which describes the random sweeping of small-scale eddies by energy-containing eddies. Consequently, the EA model achieves a successive approximation to the isocorrelation contours and has been demonstrated in many turbulent shear flows [19–21].

On the other hand, previous research has shown evidence that the wall-bounded turbulence at high Reynolds number is characterized by coherent structures of disparate scales. Specifically, in addition to the streaks and the vortical structures residing in the near-wall region [22,23], there are also large-scale motions, very-large-scale motions, and self-similar motions populating the logarithmic and outer regions [24–26]. As one of the most elegant conceptual models describing the multiscale nature of fluid motion in wall-bounded turbulence, the attached-eddy model proposed by Townsend [27] and Perry and Chong [28] hypothesizes that the logarithmic region is occupied by an array of randomly distributed and self-similar energy-containing motions (or eddies) with their roots attached to the near-wall region. Over the past decades, a growing number of studies have supported the existence of the attached eddies in wall-bounded turbulence [29–33]. For more details, we refer the reader to a recent review work by Marusic and Monty [34].

Considering that the multiscale attached eddies can penetrate deep into the near-wall region, resulting in the increment of the near-wall fluctuation intensities [35,36] and the imprint on near-wall turbulence as "footprints", also known as superposition effects [1,37–39], it would be quite natural to hypothesize that the superposition effects would affect the near-wall turbulent physical variable to some extent, such as the wall-shear fluctuation, which is a crucial physical quantity for drag generation, noise radiation, and heat transfer [40]. However, some fundamental questions may be raised, e.g., whether the superposition effects of multiscale attached eddies on near-wall turbulence account for the space-time correlation. If so, is there a corresponding Reynolds-number effect? These questions are still unanswered. In addition, since the characteristic scale of an individual attached-eddy is proportional to its wall-normal height [27,28], the examined space-time correlation in the logarithmic region using the traditional statistical approach is indeed the ensembled effects of the multiscale eddies and the space-time properties of wall-attached eddies at a given length scale is still ambiguous. For a more in-depth understanding of flow physics and to give insight into the underlying mechanisms that drive turbulent flows at different scales, the present work is dedicated to further investigating the space-time correlations of wall-shear fluctuations and streamwise velocity signals in a multiscale manner by relying on the inner-outer interaction model (IOIM) [41,42] and the attached-eddy hypothesis [27] and dissecting the direct numerical simulation (DNS) database with intensive time spanning and moderate Reynolds number.

The remainder of this paper is organized as follows. In Sec. II, the DNS database and the scale decomposition method are briefly introduced. In Sec. III, we present and evaluate the space-time correlations of wall-shear fluctuations and streamwise velocity fluctuations carried by wall-attached eddies at a given length scale. We summarize our conclusions in Sec. IV.

II. DNS DATABASE AND SCALE DECOMPOSITION METHOD

The code deployed to compute the extensively validated DNS database for channel flows [25,43–45] is utilized to generate the time-resolved channel flow data with $\mathrm{Re}_\tau = 934$ ($\mathrm{Re}_\tau = hu_\tau/\nu$, where h denotes the channel half height, u_τ is the wall friction velocity, and ν is the kinematic viscosity). The simulation is conducted in a computational domain of $8\pi h \times 3\pi h \times 2h$ with $N_x = 3072$, $N_z = 2304$, and $N_y = 385$ in the streamwise, spanwise, and wall-normal directions, respectively. The corresponding streamwise and spanwise grid resolutions in viscous units are given by $\Delta x^+ = 11.5$ and $\Delta z^+ = 5.7$, respectively. The finest and coarsest resolutions in the wall-normal direction are given by $\Delta y^+_{\min} = 0.03$ and $\Delta y^+_{\max} = 7.6$, respectively. To calculate the space-time correlation, 499 raw snapshots with a constant time interval of 0.02 are deployed. To validate the computational code and configurations deployed in this study, comparisons of the mean and root-mean-square (rms) velocity profiles with the open-source DNS database [43] are provided in Appendix A.

The decomposition of near-wall streamwise velocity fluctuation is based on the IOIM first proposed by Marusic *et al.* [41]. To avoid artificial scale decomposition, Baars *et al.* [42] modified the computational process by introducing spectral stochastic estimation, and the modified version takes the form

$$u'^+_p(y^+) = \underbrace{u^*(y^+)[1 + \Gamma_{uu} u'^+_L(y^+_o, y^+)]}_{u'^+_s} + u'^+_L(y^+_o, y^+), \tag{4}$$

in which u'^+_p denotes the predicted near-wall streamwise velocity fluctuation, u^* denotes the universal velocity signal without large-scale impact, u'^+_L is the superposition component, Γ_{uu} is the amplitude-modulation coefficient, and u'^+_s denotes the amplitude modulation of the universal signal u^*. Here u'^+_L is obtained by spectral stochastic estimation of the streamwise velocity fluctuation at the logarithmic region y^+_o, which can be expressed as

$$u'^+_L(x^+, y^+_o, y^+, z^+) = F_x^{-1}\{H_L(\lambda^+_x, y^+_o, y^+) F_x[u'^+_o(x^+, y^+_o, z^+)]\}, \tag{5}$$

where u'^+_o denotes the streamwise velocity fluctuation at ${y_o}^+$ in the logarithmic region; F_x and F_x^{-1} denote the fast Fourier transformation (FFT) and inverse FFT in the streamwise direction for one instantaneous DNS realization of the turbulent flow field, respectively; and H_L is the scale-dependent complex-valued kernel, which evaluates the coherence between $u'(y^+)$ and $u'_o({y_o}^+)$ at a given length scale λ^+_x and can be calculated as

$$H_L(\lambda^+_x, {y_o}^+, y^+) = \frac{\langle \hat{u}'(\lambda^+_x, y^+, z^+)\bar{\hat{u}}'_o(\lambda^+_x, y^+_o, z^+)\rangle}{\langle \hat{u}'_o(\lambda^+_x, y^+_o, z^+)\bar{\hat{u}}'_o(\lambda^+_x, y^+_o, z^+)\rangle}, \tag{6}$$

where $\hat{u}'$ is the Fourier coefficient of u' and $\bar{\hat{u}}'_o$ is the complex conjugate of $\hat{u}'_o$.

In this work, we mainly focus on the streamwise velocity fluctuation generated by the wall-attached eddies in the logarithmic region. Thus, the predicted near-wall position y^+_w is set as $y^+_w = 0.03$ and the outer reference height ${y_o}^+$ varies from $y^+ = 100$ (denoted by $y^+_{o,s}$) to $0.2h^+$ (denoted by $y^+_{o,e}$), i.e., the lower and upper boundaries of the logarithmic region [46]. According to the hierarchical energy-containing eddies in high-Reynolds-number wall turbulence [34] (as shown in Fig. 2), an array of wall-attached eddies with distinct wall-normal heights can convect simultaneously past this reference position ${y_o}^+$ and the calculated signal $u'^+_L(x, {y_o}^+, y^+_w, z)$ in Eq. (5) represents the superposition contributed from the wall-coherent eddies with their heights larger than ${y_o}^+$; detached eddies cannot contribute to it since the necessary interaction with the wall is absent. Consequently, the superposition component of streamwise wall-shear stress fluctuation ε'^+_x can be calculated by definition, i.e., $\partial u'^+_L(x, {y_o}^+, y^+_w, z)/\partial y^+$ at the wall, and is denoted by $\varepsilon'^+_{x,L}(y^+_o)$.

III. RESULTS AND DISCUSSION

A. Space-time correlations of wall-shear fluctuations due to the Reynolds-number effect

Previous studies [47,48] verified that the generation of wall-shear stress fluctuations can be considered as the additive outcomes of the momentum cascade across momentum-carried eddies of different scales, and the amplification of the corresponding inner-outer interactions as the Reynolds number increases is typically attributed to the growing large-scale eddies populating the logarithmic and outer regions [36,49]. Combined with the numerical framework in the preceding section, the difference value $\Delta\varepsilon'^+_x({y_o}^+) = \varepsilon'^+_x - \varepsilon'^+_{x,L}(y^+_o)$ can be further interpreted as the accumulation of the superposition generated by the wall-coherent eddies with their wall-normal heights smaller than ${y_o}^+$ and the contribution of the near-wall small-scale motions. When increasing the outer reference location ${y_o}^+$, more and more large-scale energy-containing eddies populating the logarithmic region

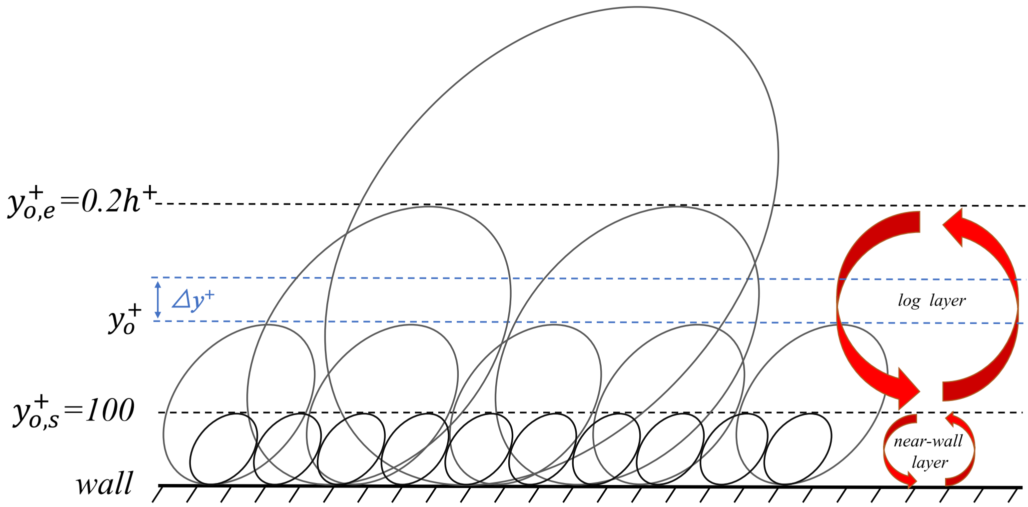

FIG. 2. Sketch of the multiscale analysis for wall turbulence [30]. Each circle represents an individual attached eddy. Here y_s^+ ($y^+ = 100$) and y_e^+ ($0.2h^+$) denote the lower and upper bounds of the logarithmic region, respectively, y_o^+ is the outer reference height, and Δy^+ is the local grid spacing in the wall-normal direction.

will be incorporated by $\Delta\varepsilon_x'^+(y_o{}^+)$, which is in line with the effect of increasing the Reynolds number. Considering that the normalized outer reference height $y_o^+ = y_o/\delta_\nu = y_o u_\tau/\nu = y_o \mathrm{Re}_\tau/h$ can be interpreted as the local Re_τ, the increase of $y_o{}^+$ corresponds to the enlargement of the local Re_τ. In this way, the Reynolds-number effect on the space-time correlation of wall-shear fluctuations can be estimated directly.

To demonstrate the scale characteristics of $\Delta\varepsilon_x'^+(y_o{}^+)$ for different wall-normal heights $y_o{}^+$, Fig. 3 shows the premultiplied spectra of $\Delta\varepsilon_x'^+(y_o{}^+)$. To facilitate the comparison, the spectrum of wall-shear stress fluctuations $\varepsilon_x'^+$ is also included [denoted by $k_x\phi^+$, where ϕ^+ stands for the

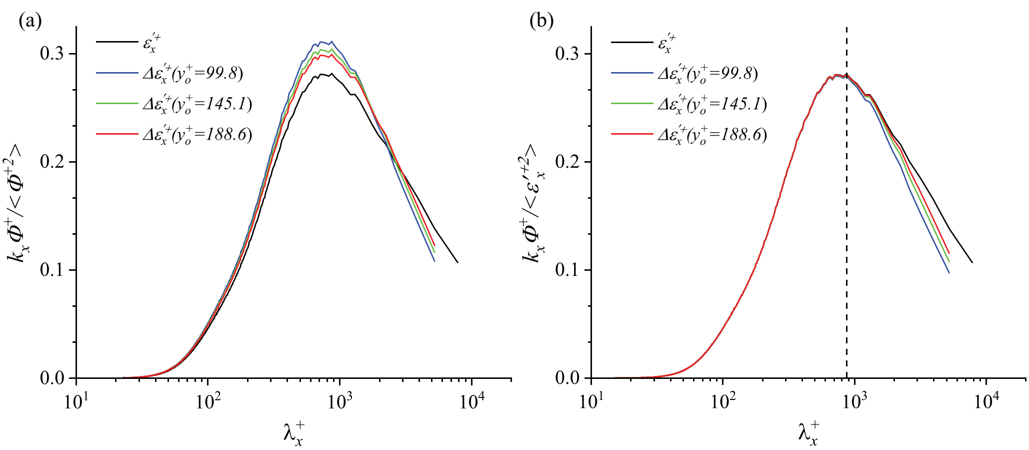

FIG. 3. Streamwise premultiplied spectra of streamwise wall-shear stress fluctuations $\varepsilon_x'^+$ and the difference value $\Delta\varepsilon_x'^+(y_o{}^+)$ for $y_o{}^+ = 99.8$, 145.1, and 188.6. The spectra are normalized by (a) the corresponding intensity and (b) the energy of $\varepsilon_x'^+$. The vertical dashed line denotes the characteristic length scales of the near-wall turbulence [50,51].

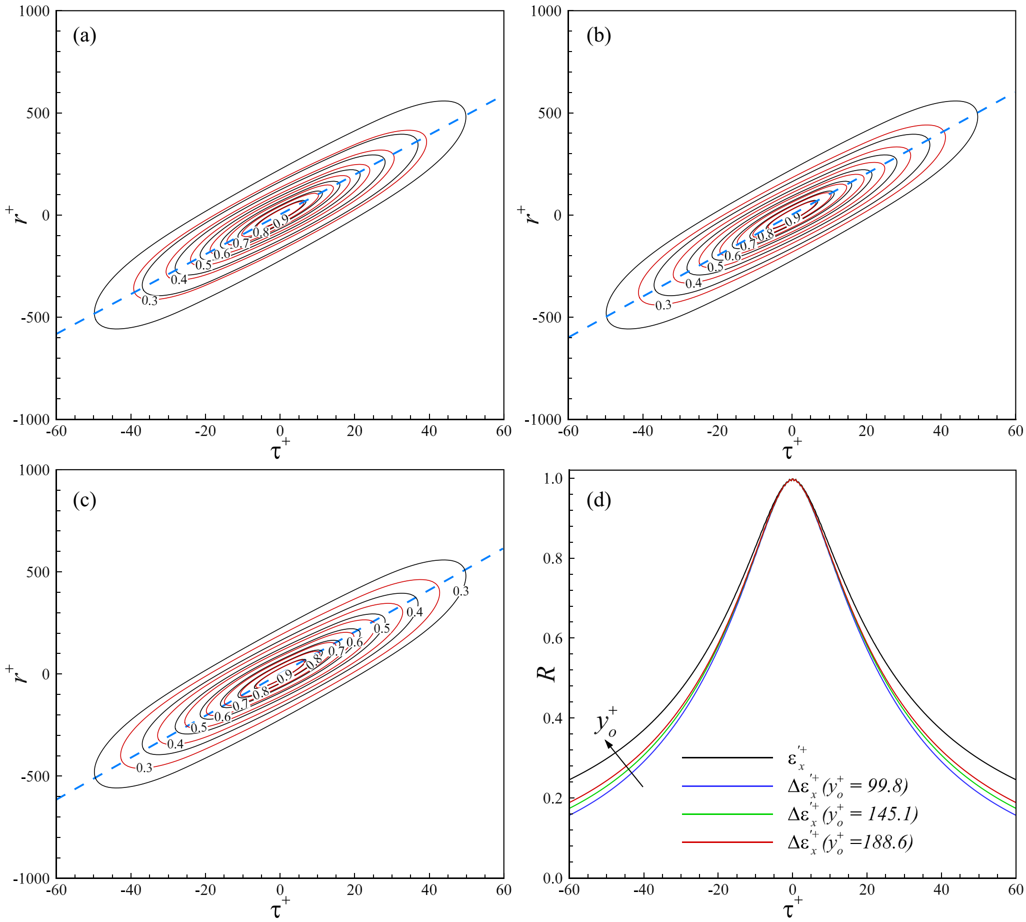

FIG. 4. Contours of space-time correlations as a function of space separation and time delay for $\varepsilon_x'^+$ (black) and $\Delta\varepsilon_x'^+(y_o{}^+)$ (red) at (a) $y_o^+ = 99.8$, (b) $y_o^+ = 145.1$, and (c) $y_o^+ = 188.6$. The contour levels are equally spaced from 0.3 to 0.9 with increments of 0.1. (d) Space-time correlation R as a function of time delay along the preference direction (blue dashed line).

energy for specific streamwise wave number k_x, with both ϕ^+ and k_x calculated by the FFT of the signal φ^+, which can be $\varepsilon_x'^+$ or $\Delta\varepsilon_x'^+(y_o{}^+)$] and each spectrum in Fig. 3(a) is normalized by its corresponding intensity. It is apparent that the relative energy proportion of small length scales in $\Delta\varepsilon_x'^+(y_o{}^+)$ increases as the outer reference height $y_o{}^+$ decreases, whereas for the large length scales, the contrary is the case. This scenario is consistent with the expectation that more and more superposition components generated by the large-scale wall-coherent eddies with their heights larger than $y_o{}^+$ will be removed as the outer reference height $y_o{}^+$ decreases. Furthermore, when the energy spectra are normalized by the energy of $\varepsilon_x'^+$, as shown in Fig. 3(b), the spectral curves with length scales smaller than $\lambda_x^+ \approx 1000$, i.e., the well-documented spectral scale characteristics of the near-wall turbulence and streaks, almost overlap with each other. This observation highlights the fact that the aforementioned numerical methodology does not disturb the near-wall small-scale structures. Additionally, the energy distribution for large length scales in $\Delta\varepsilon_x'^+(y_o{}^+)$ gradually approaches that of $\varepsilon_x'^+$ as the reference location $y_o{}^+$ increases, which also demonstrates the feasibility of inspecting the Reynolds-number effect with the signal $\Delta\varepsilon_x'^+(y_o{}^+)$.

Figures 4(a)–4(c) show the contours of space-time correlations as a function of space separation and time delay for the $\Delta\varepsilon_x'^+({y_o}^+)$ with the inputs of three selected wall-normal positions ${y_o}^+$ in the logarithmic region and compared with that for the full streamwise wall-shear stress fluctuations $\varepsilon_x'^+$. Other wall-normal positions in the logarithmic region have similar characteristics and are not shown here for brevity. It can be seen that the isocorrelation contours show approximately elliptical shapes instead of straight lines, and the space-time correlations reach a maximum at the origin and decay with increasing separations in space and/or time. To illustrate vividly the variation of space-time correlations, Fig. 4(d) displays the space-time correlations in the preference direction, i.e., the direction with the slowest decay rate [shown by the blue dashed line in Figs. 4(a)–4(c)], as a function of the time delay. It can be seen that for the central regions with strong correlation, where $R > 0.8$, the space-time correlations of $\Delta\varepsilon_x'^+({y_o}^+)$ with the inputs of different wall-normal positions ${y_o}^+$ have morphological characteristics virtually identical to the full channel data $\varepsilon_x'^+$ and the decaying rates of correlations in the preference direction are roughly synchronous. This underscores the fact that the wall-shear stress fluctuation with strong space-time correlations is mainly dominated by near-wall small-scale motions, and the Reynolds-number effect can be neglected. For the weakly correlated regions with large space separations and/or time delays, where $R < 0.8$, the decaying rate of space-time correlations decreases monotonically as the wall-normal location ${y_o}^+$ increases and the isocorrelation contours concurrently move closer to the full channel data. This implies that the space-time correlations of wall-shear fluctuations are amplified as the local Reynolds number increases, which is typically attributed to the magnitude increase of the footprint for wall-attached eddies in the logarithmic region. Furthermore, this monotonic variation highlights that the superpositions of wall-attached logarithmic-region motions on the wall surface follow the additive process, which is consistent with the well-documented attached-eddy hypothesis.

To further dissect the statistical characteristics, Fig. 5(a) shows the comparison of the convection velocities for $\varepsilon_x'^+$ and $\Delta\varepsilon_x'^+({y_o}^+)$ with the inputs of different wall-normal positions ${y_o}^+$. Following previous research [52,53], the overall convection velocity U_c is defined as

$$U_c = \arg\max_U F(U), \quad F(U) = \int_{-\infty}^{+\infty} R(U\tau, \tau) d\tau, \tag{7}$$

which achieves the maximum value for the integrated space-time correlation. Additionally, Figs. 5(b) and 5(c) display the convection velocity U and sweeping velocity V, respectively, defined by the EA model $R(r,\tau) = R[\sqrt{(r-U\tau)^2 + V^2\tau^2}, 0]$. It can be observed that the magnitudes of both convection velocities U_c and U increase monotonically as ${y_o}^+$ increases and gradually approach the convection velocity of full channel data $\varepsilon_x'^+$. This observation can also be explained through the hierarchical organization of wall-attached eddies in high-Reynolds-number wall turbulence. Specifically, the increase of ${y_o}^+$ indicates that $\Delta\varepsilon_x'^+({y_o}^+)$ will be contributed by more and more superposition effects generated by high-speed logarithmic eddies with their wall-normal heights smaller than ${y_o}^+$. In this way, this scenario indicates that the amplification of the inner-outer interactions as the Reynolds number increases not only increases the magnitude of the fluctuation intensity [36] but also can accelerate the convection velocity of small-scale turbulence motions in the near-wall region. In contrast, for the sweeping velocity V, which describes the random sweeping of small-scale eddies, the corresponding value is not affected visibly with the increment of the local Reynolds number.

In addition, it is instructive to compare the geometric parameters of the space-time correlation contours for $\varepsilon_x'^+$ and $\Delta\varepsilon_x'^+({y_o}^+)$ with the inputs of different wall-normal positions, such as the lengths of the major axis and the minor axis for specific contour levels (denoted by a and b in Fig. 1, respectively). Figure 5(d) shows the length of a major axis as a function of the length of a minor axis for three selected wall-normal positions ${y_o}^+$. It can be seen that the length of the main axis almost increases linearly with the length of the minor axis within the range of $a^+ < 15$; the corresponding slope, known as the aspect ratio, is approximately equal to a constant, which is consistent with the main hypothesis of the EA model as stated by He and Zhang [16]. For space-time correlation

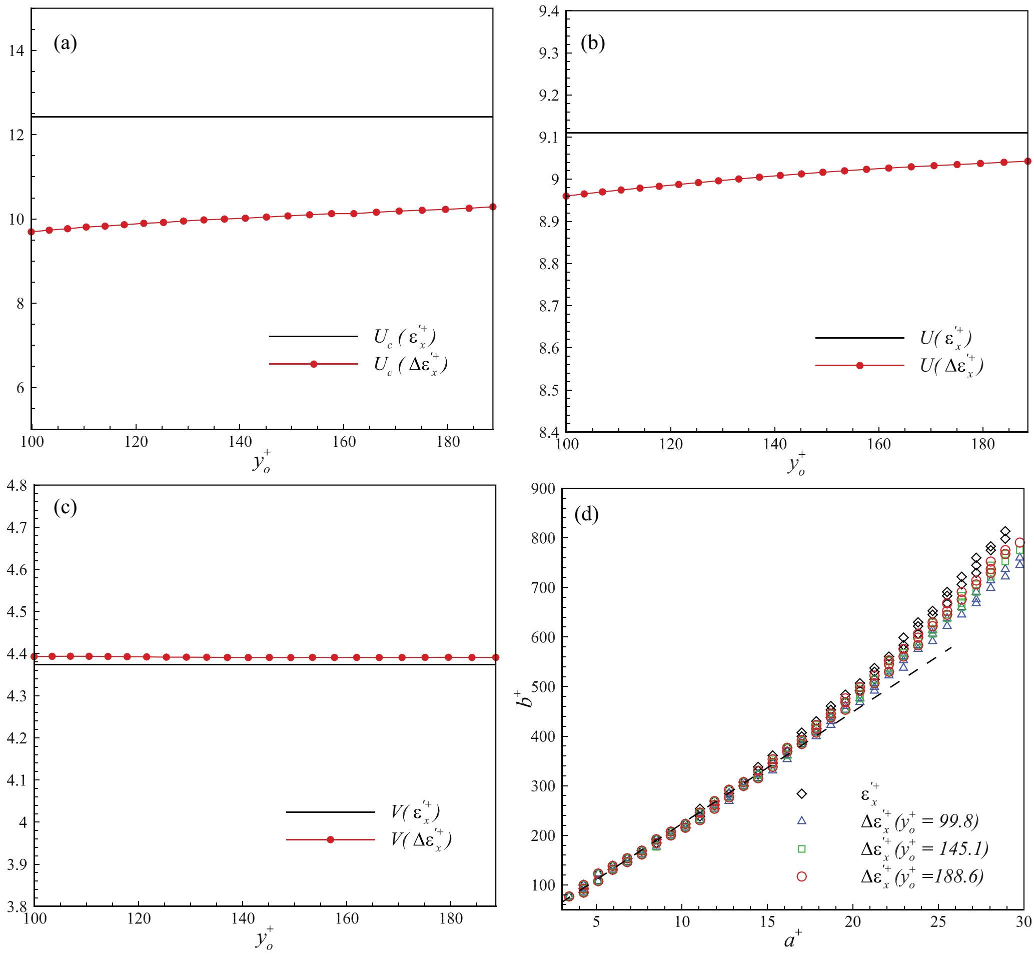

FIG. 5. Variations of (a) overall convection velocity U_c, (b) convection velocity U, and (c) sweeping velocity V defined by the EA model for $\varepsilon_x'^{+}$ (black) and $\Delta\varepsilon_x'^{+}(y_o{}^{+})$ (red) as a function of the wall-normal position $y_o{}^{+}$. (d) Length of the major axis as a function of the length of the minor axis for the contours of $\varepsilon_x'^{+}$ and $\Delta\varepsilon_x'^{+}(y_o{}^{+})$ at three selected wall-normal positions $y_o{}^{+}$.

contours with a larger axis length, slight monotonic discrepancies are observed with the increment of wall-normal position $y_o{}^{+}$, indicating that the increase of local Reynolds number will change the geometric characteristics of contours to a larger aspect ratio and the corresponding space-time correlation is amplified in the preference direction in a monotonic manner. Other wall-normal positions bear similar results and are not shown here for brevity.

B. Space-time correlation of streamwise velocity fluctuation in the logarithmic region

Before studying the streamwise velocity fluctuation with the multiscale analysis, it is better to have an overall picture of the ensembled space-time correlations in the logarithmic region. Figure 6 shows the contours of space-time correlations as a function of space separation and time delay for the streamwise velocity fluctuation at four selected wall-normal positions in the logarithmic region. It can be observed that these contours are clustered in a thin band, which implies the strong convective nature of the streamwise velocity fluctuation in the logarithmic region. Additionally, the slopes of the preference directions become large with increasing wall-normal location (to be specific,

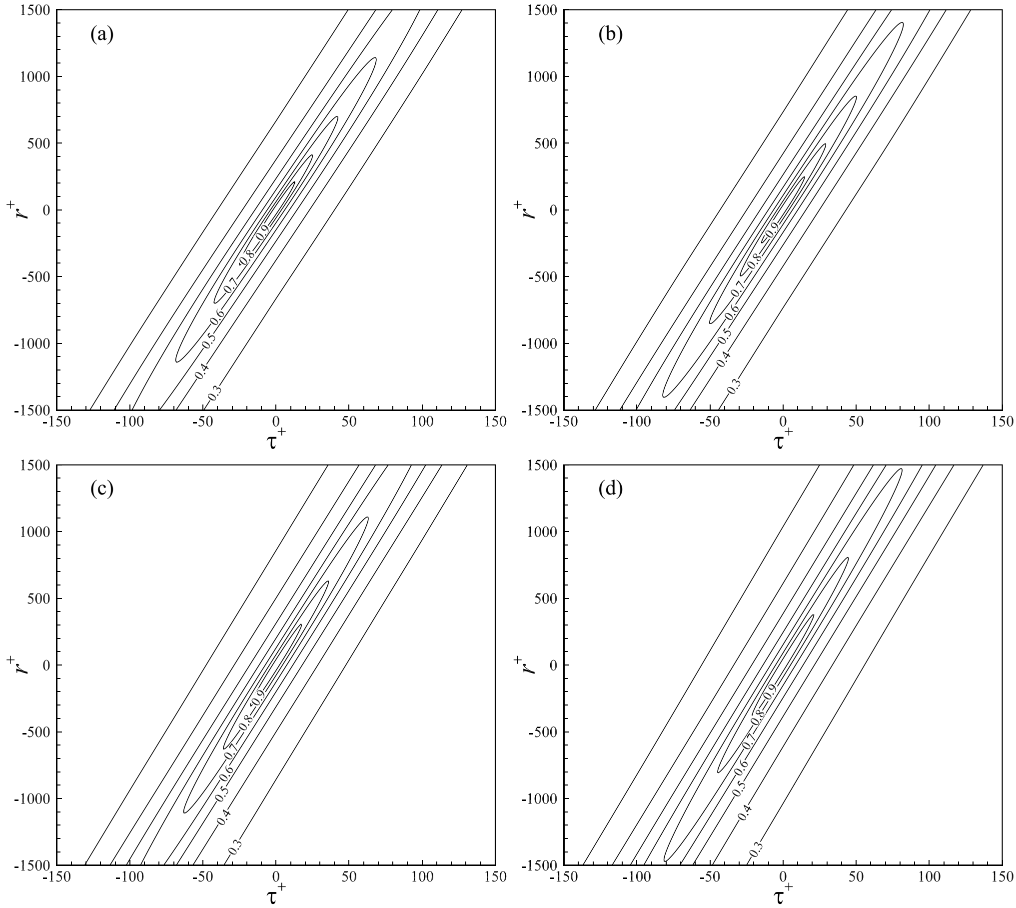

FIG. 6. Contours of space-time correlations as a function of space separation and time delay for the streamwise velocity fluctuation $u'^+(y^+)$ at (a) $y^+ = 99.8$, (b) $y^+ = 121.5$, (c) $y^+ = 153.4$, and (d) $y^+ = 188.6$. The contour levels are equally spaced from 0.3 to 0.9 with increments of 0.1.

$U_{c,(y^+=99.8)} = 16.69$, $U_{c,(y^+=121.5)} = 17.11$, $U_{c,(y^+=153.4)} = 17.67$, and $U_{c,(y^+=188.6)} = 18.14$), which is consistent with the variation tendency of the mean streamwise velocity.

Figure 7 plots the evolution of the space-time correlations R with respect to the time separation τ^+ and the separation $r_{\mathrm{EA}} = \sqrt{(r - U\tau)^2 + V^2\tau^2}$ defined by the EA model for different space separations $r^+ = 0$, 145.4, 298.4, 451.5, 604.6, 757.6 at the locations $y^+ = 99.8$ and 188.6. Here the parameters U and V are calculated from the DNS data [16]. For $y^+ = 99.8$ and 188.6, (U, V) are calculated as (16.01,2.33) and (17.67,2.09), respectively. It can be seen that the normalization defined by the EA model causes an excellent collapse for the correlation curves at different space separations with that at zero space separation, i.e., $r^+ = 0$. This observation signifies that the EA model provides a feasible interpretation for the decorrelation process of the ensembled space-time properties of logarithmic motions. Other locations yield similar results and are not shown here for brevity.

For a more in-depth understanding of the space-time properties of attached eddies at a given length scale, we can also use the streamwise velocity fluctuation in the near-wall position y_w^+ as the input signal to reconstruct the wall-coherent streamwise velocity fluctuation in the logarithmic

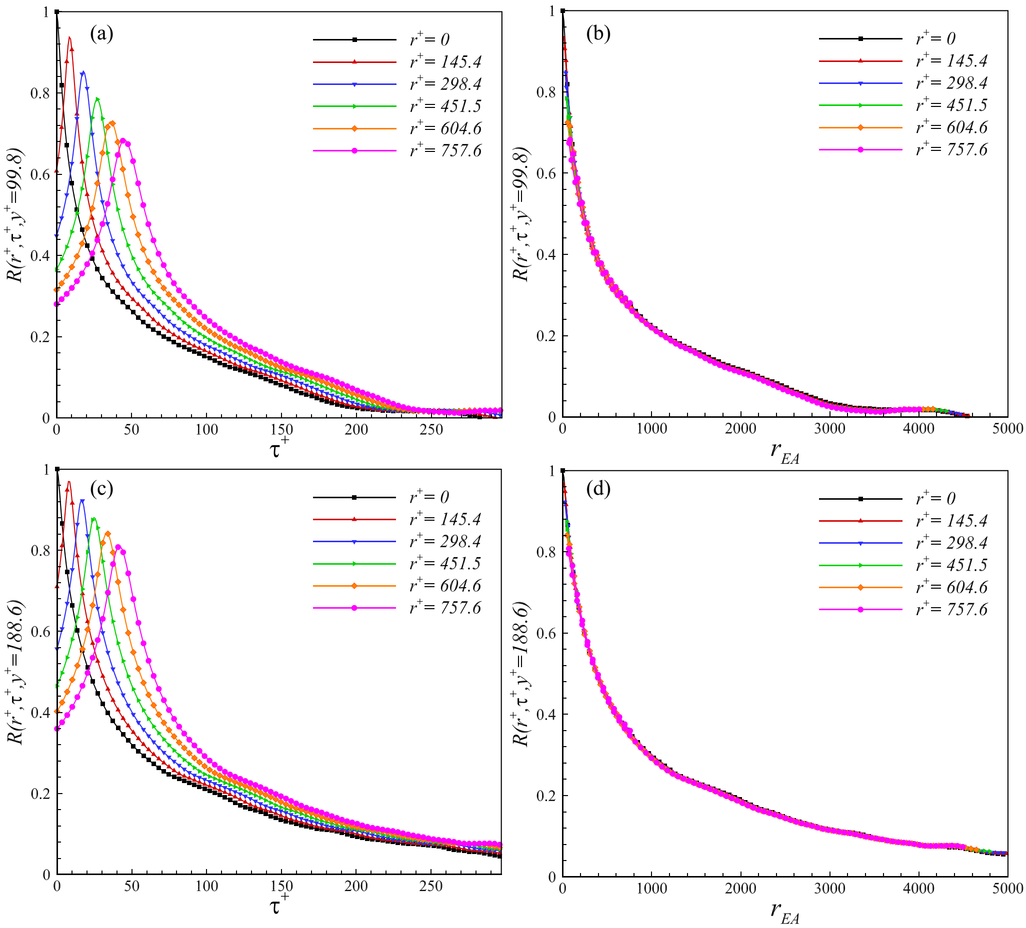

FIG. 7. Space-time correlations R at (a) and (b) $y^+ = 99.8$ and (c) and (d) $y^+ = 188.6$ for different space separation r^+ plotted against (a) and (c) the time separation τ^+ and (b) and (d) the separation $r_{\mathrm{EA}} = \sqrt{(r - U\tau)^2 + V^2\tau^2}$ defined by the EA model.

region y_o^+ by spectral stochastic estimation [54], i.e.,

$$u_W'^+(x^+, y_w^+, y_o^+, z^+) = F_x^{-1}\{H_W(\lambda_x^+, y_w^+, y_o^+)F_x[u'^+(x^+, y_w^+, z^+)]\}, \tag{8}$$

where $u_W'^+$ is the wall-coherent component of $u_o'^+$ and can be considered approximately the streamwise velocity fluctuations carried by the wall-attached eddies with their height larger than y_o^+ [55]. The input near-wall position y_w^+ is set as 0.03 in this study and the statistic sensitivity to the choice of y_w^+ is examined in Appendix B. The wall-based transfer kernel H_W can be calculated as

$$H_W(\lambda_x^+, y_w^+, y_o^+) = \frac{\langle \hat{u}_o'(\lambda_x^+, y_o^+, z^+)\hat{\bar{u}}'(\lambda_x^+, y_w^+, z^+)\rangle}{\langle \hat{u}'(\lambda_x^+, y_w^+, z^+)\hat{\bar{u}}'(\lambda_x^+, y_w^+, z^+)\rangle}. \tag{9}$$

According to the hierarchical distribution of the multiscale wall-attached eddies in high-Reynolds-number wall turbulence (see Fig. 2), the difference value $\Delta u_W'^+({y_o}^+) = u_W'^+({y_o}^+) - u_W'^+({y_o}^+ + \Delta y^+)$ can be interpreted as the streamwise velocity fluctuation carried by wall-attached eddies populating the region between y_o^+ and ${y_o}^+ + \Delta y^+$, where ${y_o}^+ + \Delta y^+$ represents the location of the wall-normal grid cell adjacent to that at y_o^+, and Δy^+ is the local grid spacing in the wall-normal direction, in viscous units, which is a simulation-defined parameter.

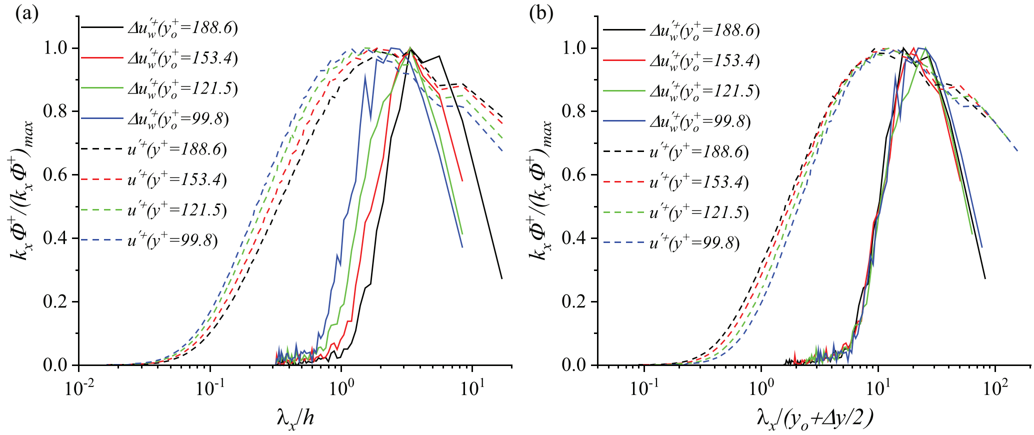

FIG. 8. Streamwise premultiplied spectra of $u'^+(y^+)$ and $\Delta u_W'^+(y_o{}^+)$ as a function of (a) λ_x/h and (b) $\lambda_x/(y_o+\Delta y/2)$ at four selected wall-normal positions. Each spectrum is normalized with its maximum value.

To investigate further the scale characteristics, Fig. 8 shows the premultiplied spectra of $\Delta u_W'^+(y_o{}^+)$ for different wall-normal locations. The spectra of streamwise velocity fluctuation $u'^+(y^+)$ from full-channel data are also included for comparison. Each spectrum is normalized with its maximum value. It can be seen from Fig. 8(a) that the energy distributions of $\Delta u_W'^+(y_o{}^+)$ are more concentrated in large length scales compared to the full-channel data u'^+ and the corresponding streamwise length scales of the dominant spectral curve increase with $y_o{}^+$, which is in accordance with the energy fraction captured by the attached-eddy model [56,57]. In addition, since the statistical characteristics of an individual attached eddy are self-similar with its wall-normal height as per the attached-eddy hypothesis [27], Fig. 8(b) displays the variations of streamwise premultiplied spectra as a function of $\lambda_x/(y_o+\Delta y/2)$, i.e., the characteristic scale of the wall-attached motions within y_o and $y_o+\Delta y$. It can be seen that the profiles of $\Delta u_W'^+(y_o{}^+)$ for all wall-normal locations collapse with each other. This observation also supports the viewpoint put forward above that the $\Delta u_W'^+(y_o{}^+)$ signals are the streamwise velocity fluctuations carried by the self-similar attached eddies at the specific characteristic length scale.

Figure 9 compares the contours of space-time correlations as a function of space separation and time delay for $\Delta u_W'^+(y_o{}^+)$ at four selected wall-normal positions $y_o{}^+$ in the logarithmic region. Other wall-normal positions in the logarithmic region have similar characteristics and are not shown here for brevity. It can be seen that the space-time correlations of streamwise velocity fluctuations carried by attached eddies at a given length scale feature distinctly different contours from those illustrated in Fig. 6. They are more like wide elliptical shapes in alignment with the preference direction. To characterize quantitatively the difference of geometric parameters, Fig. 10(a) plots the length of the major axis as a function of the length of the minor axis for $u'^+(y^+)$ and $\Delta u_W'^+(y_o{}^+)$ at four selected wall-normal positions. It can be observed that the space-time correlation contours for attached eddies at a given length scale display a different self-similarity property, as evidenced by the fact that the corresponding aspect ratios are much smaller than those of ensembled space-time correlation with strong convective nature. Additionally, Fig. 10(b) shows the variations of convection velocity U_c for $\Delta u_W'^+(y_o{}^+)$ as a function of the wall-normal position $y_o{}^+$. In conjunction with Fig. 9, it can be seen that both the counter area for a specific correlation and the advection velocity increase as the wall-normal position $y_o{}^+$ increases. This observation underscores the fact that attached eddies with larger characteristic scales feature not only larger spatial structures but also a longer lifetime. Furthermore, as the characteristic scale increases, the corresponding convection velocity of the attached eddies also gradually increases, remaining at approximately 93% of the

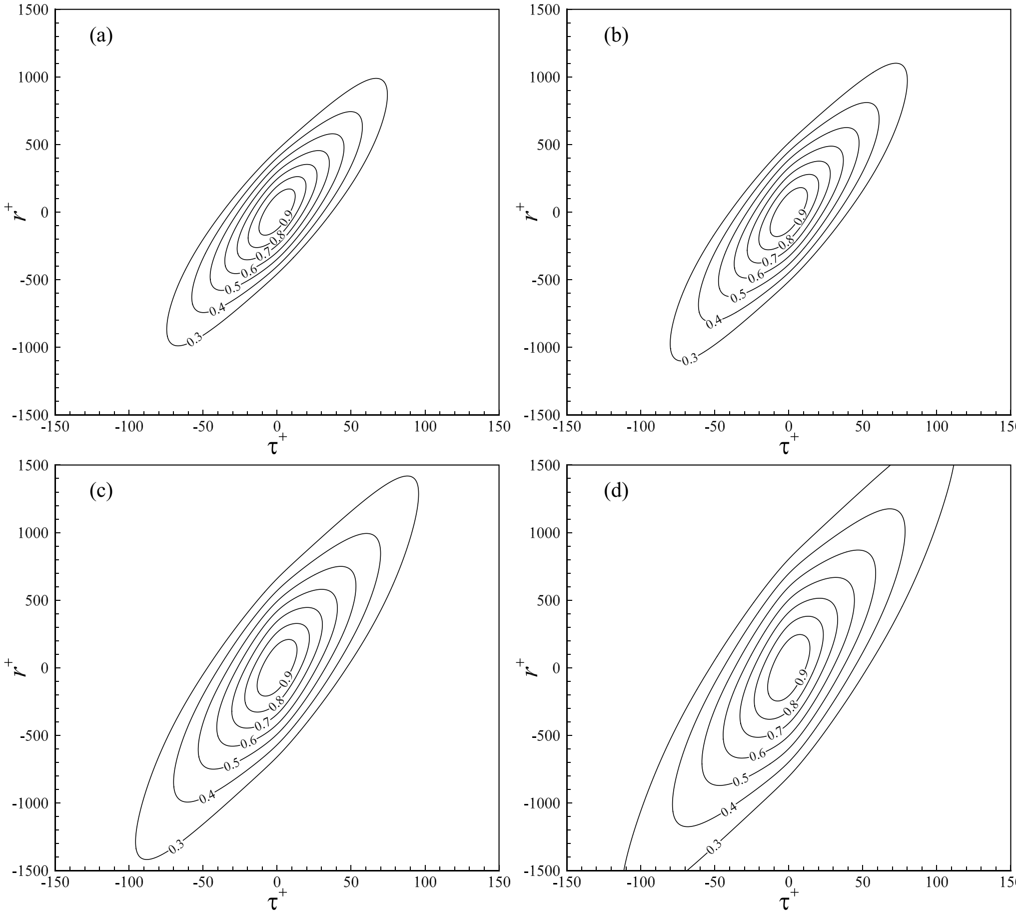

FIG. 9. Contours of space-time correlations as a function of space separation and time delay for $\Delta u_W'^+(y_o{}^+)$ at (a) $y_o^+ = 99.8$, (b) $y_o^+ = 121.5$, (c) $y_o^+ = 153.4$, and (d) $y_o^+ = 188.6$. The contour levels are equally spaced from 0.3 to 0.9 with increments of 0.1.

local mean streamwise velocity. The Reynolds-number effect on the presented results is examined in Appendix C.

IV. CONCLUSION

In the present study we investigated the space-time correlations of both wall-shear fluctuations and the streamwise velocity fluctuations carried by wall-attached eddies at a given length scale in a multiscale manner, by coupling the IOIM with the attached-eddy hypothesis. The conclusions are summarized as follows.

(i) The wall-shear stress fluctuations with strong space-time correlations are mainly dominated by near-wall small-scale motions and the Reynolds-number effect can be neglected. For the weakly correlated regions with large space separations and/or time delays, the corresponding space-time correlations are amplified in a self-similar manner with increasing local Reynolds number as a result of the superposition effects of wall-attached eddies in the logarithmic region.

(ii) The EA model, which accounts for the shearing of mean flows and random sweeping of velocity fluctuations in the logarithmic region via a second-order approximation to the isocorrelation contours, leads to an excellent collapse of ensembled space-time correlations in the present database

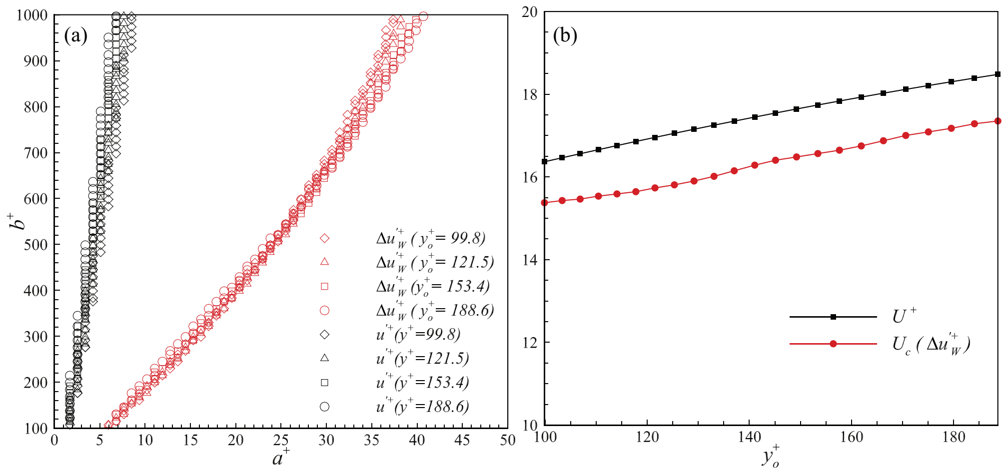

FIG. 10. (a) Length of the major axis as a function of the length of the minor axis for $u'^+(y^+)$ and $\Delta u_W'^+(y_o{}^+)$ at four selected wall-normal positions. (b) Variation of the mean streamwise velocity U^+ (black) and overall convection velocity U_c for $\Delta u_W'^+(y_o{}^+)$ (red) as a function of the wall-normal position $y_o{}^+$.

at high-Reynolds number. However, the space-time correlation contour of streamwise velocity fluctuation carried by attached eddies at a given length scale exhibits a distinctly different self-similarity property as compared to that of ensembled space-time correlation with strong convective nature. The characteristic scale dependence of space-time correlation of these eddies should be accounted for by an advanced model in this sense. Our results further reveal that wall-attached eddies with larger characteristic scales feature a longer lifetime and larger convection velocity, which remains at approximately 93% of the local mean streamwise velocity.

Considering the wall-modeled large-eddy simulation (WMLES), which models the near-wall underresolved small-scale turbulent motions with the Reynolds-averaged Navier-Stokes (RANS) model while resolving the turbulence scales above the grid spacing in the outer boundary layer with large-eddy simulation (LES), is believed to be the next-generation high-fidelity simulation tool when compared to the RANS and DNS methods, the numerical framework deployed in this study may pave a way for analyzing the space-time properties for different flow scales and optimizing the modeling capability of WMLES to the interrelated problems. To be specific, it is well known that the solution quality from the WMLES approach heavily depends on the deployed LES subgrid-scale (SGS) model and the numerical scheme as well as the wall model. Different combinations of the SGS model and the numerical method may result in huge cross-code uncertainties, even when the same state-of-the-art wall model is adopted. The conventional choice in terms of combining different numerical schemes, SGS models, and the near-wall models is generally based on the metrics of replicating the mean flow statistics [58,59], without giving sufficient credit to the space-time properties of the different turbulence scales, which are important for high-order turbulence statistics or acoustic noise prediction. In order to develop the optimal WMLES framework that not only delivers accurate mean flow statistics but also predicts reliable space-time statistics with different flow scales, the present multiscale analysis of the space-time correlation can serve as a potential option to diagnose the performance of one specific WMLES framework.

ACKNOWLEDGMENTS

L.F. acknowledges financial support from the Research Grants Council (RGC) of the Government of Hong Kong Special Administrative Region (HKSAR) through RGC/ECS (Project No. 26200222), RGC/GRF (Project No. 16201023), and RGC/STG (Project No. STG2/E-605/23-N);

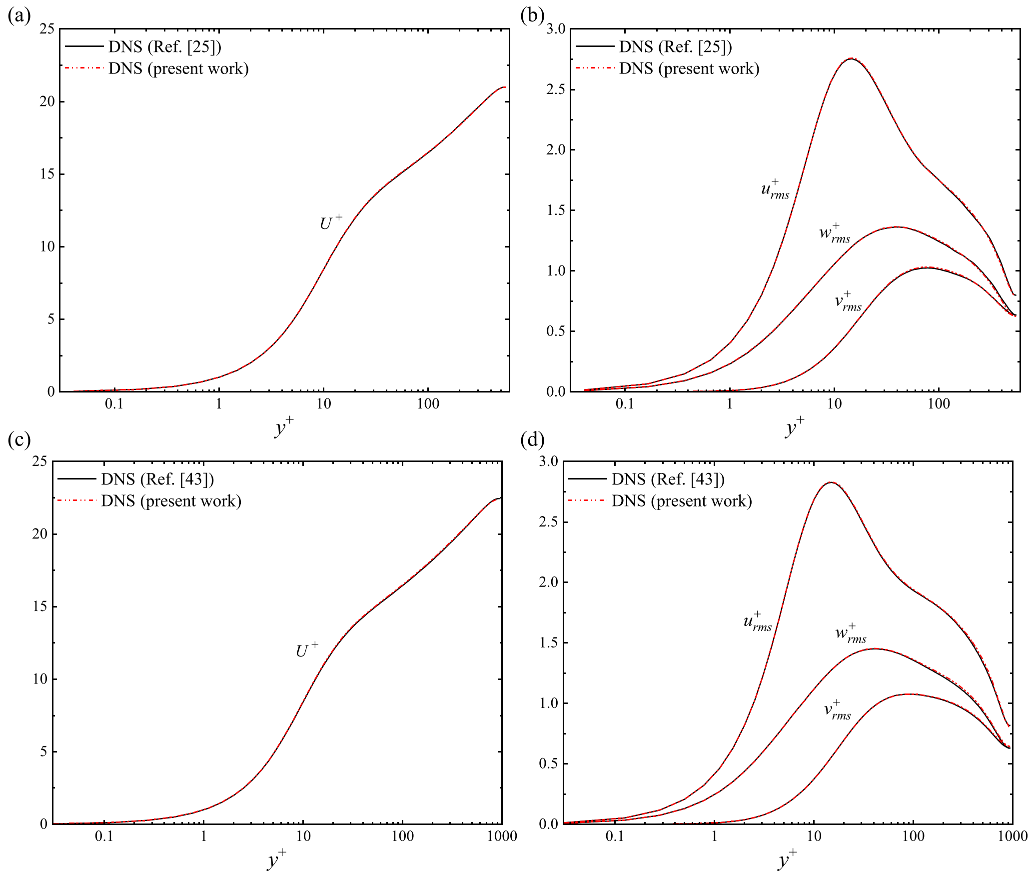

FIG. 11. Comparisons of the mean and rms profiles between the DNS database generated by the code deployed in this study and the open-source DNS results [25,43] for (a) and (b) $\mathrm{Re}_\tau = 547$ and (c) and (d) $\mathrm{Re}_\tau = 934$.

from Guangdong Basic and Applied Basic Research Foundation; from Guangdong Province Science and Technology Plan (Project No. 2023A0505030005); from CORE as a joint research center for ocean research between Laoshan Laboratory and HKUST; from the Hetao Shenzhen-Hong Kong Science and Technology Innovation Cooperation Zone (Project No. HZQB-KCZYB-2020083).

APPENDIX A: VALIDATION OF THE DNS CODE AND CONFIGURATIONS

In Fig. 11 the DNS database generated by the code deployed in this study is compared with the open-source DNS database [25,43] for the mean streamwise velocity and the rms velocities. To obtain statistically convergent results, the normalized total simulation time $u_\tau T/h$ is increased to 5.0 in each case. It can be seen that the discrepancy between the statistics of the two data sets is negligible, which demonstrates that the DNS data generated in this study are reliable.

APPENDIX B: STATISTIC SENSITIVITY TO THE INPUT NEAR-WALL POSITION y_w^+

The influence of the input near-wall position y_w^+ for calculating space-time correlations is examined. Figures 12(a), 12(b) and 12(c), 12(d) show the contours of space-time correlations as a function of space separation and time delay for $\Delta u_W'^+(y_o{}^+)$ with input near-wall position $y_w^+ = 1.12$ in the viscous sublayer and $y_w^+ = 10.12$ in the buffer layer, respectively. To facilitate the comparison,

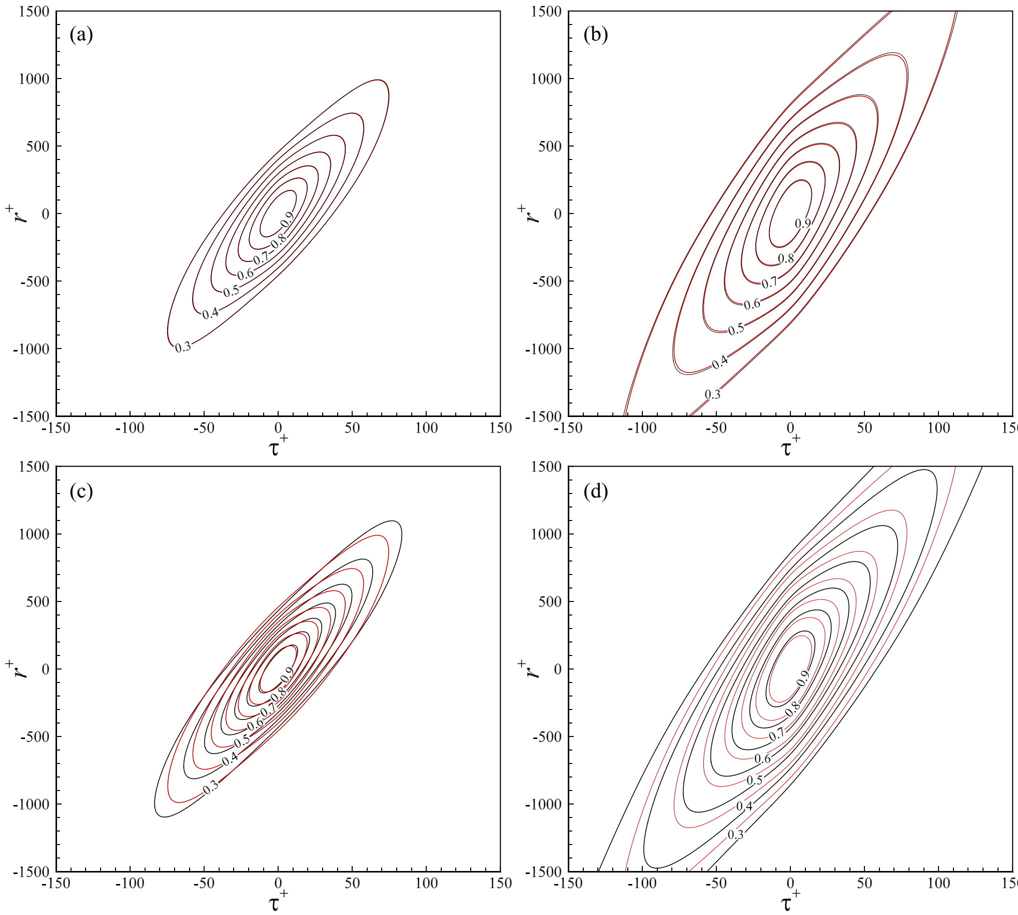

FIG. 12. Contours of space-time correlations as a function of space separation and time delay for $\Delta u_W^{\prime +}({y_o}^+)$ with the input near-wall position (a) and (b) $y_w^+ = 1.12$ in the viscous sublayer and (c) and (d) $y_w^+ = 10.12$ in the buffer layer at (a) and (c) $y_o^+ = 99.8$ and (b) and (d) $y_o^+ = 188.6$. The red lines denote the corresponding results with $y_w^+ = 0.03$ deployed in this study. The contour levels are equally spaced from 0.3 to 0.9 with increments of 0.1.

the corresponding results with $y_w^+ = 0.03$ deployed in this study are also included and marked as red lines.

The space-time correlation contours in Figs. 12(c) and 12(d) display a noticeable deviation as the input near-wall position shifts to the buffer layer with $y_w^+ = 10.12$, whereas for the input near-wall position $y_w^+ = 1.12$ in the viscous sublayer, the deviation is negligible. This observation is reminiscent of the property of coherent detached eddies that are also capable of interacting with the near-wall turbulence. To be specific, the increase of y_w^+ leads to a larger fractional contribution from coherent detached eddies to $\Delta u_W^{\prime +}({y_o}^+)$ rather than just the contribution from the attached eddies at a given length scale which is of interest to us. We have also checked that as long as the input position is around $y_w^+ < 1$, the results put forward above are insensitive to the choice of specific y_w^+.

APPENDIX C: SPACE-TIME CORRELATIONS OF STREAMWISE VELOCITY FLUCTUATION FOR CHANNEL FLOW WITH $\mathrm{Re}_\tau = 547$

To further demonstrate the Reynolds-number effect on the space-time correlations of streamwise velocity fluctuation carried by wall-attached eddies at a given length scale, the time-resolved DNS

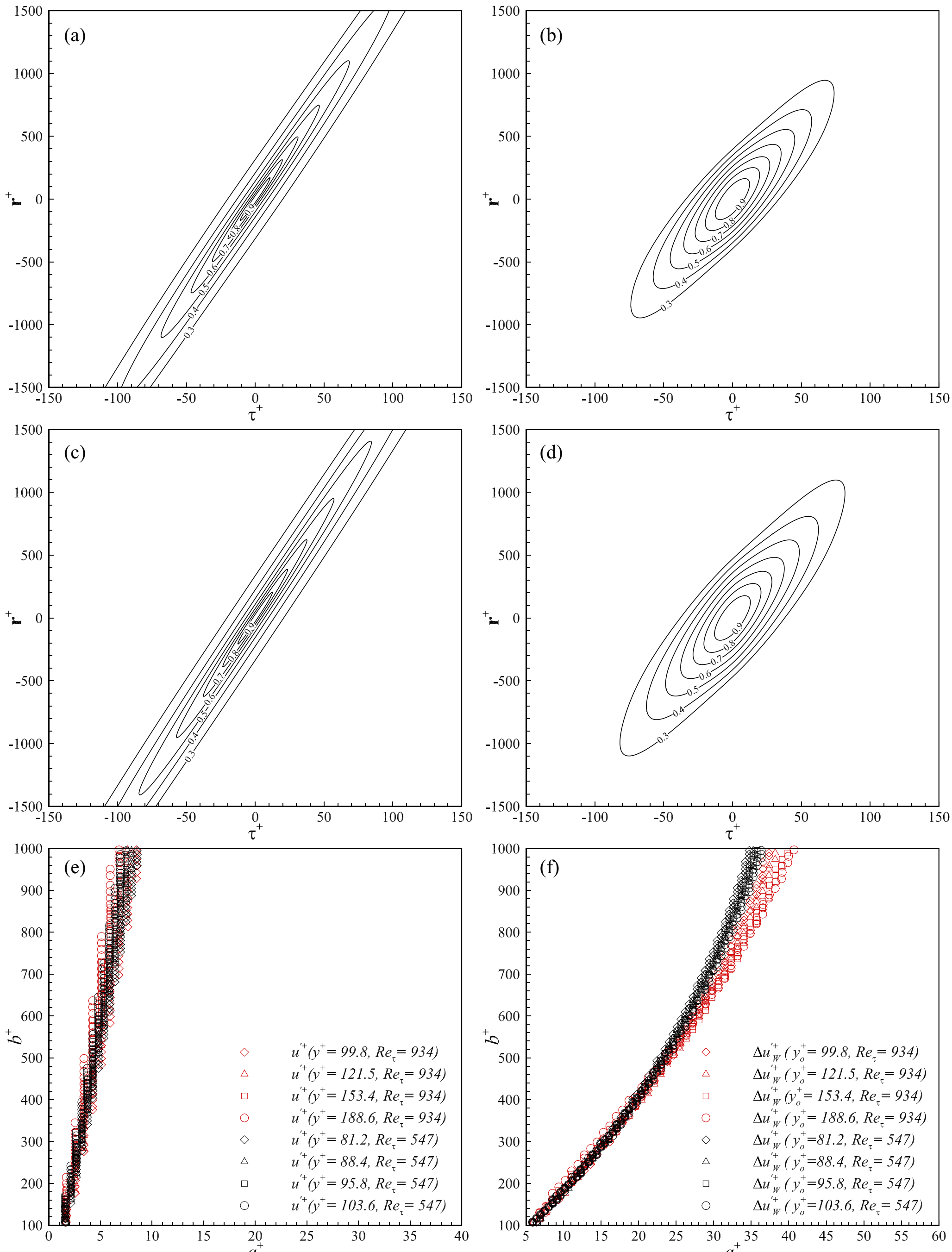

FIG. 13. Contours of space-time correlations as a function of space separation and time delay for (a) and (c) the streamwise velocity fluctuation $u'^{+}(y^{+})$ and (b) and (d) $\Delta u_W'^{+}(y_o{}^{+})$ at two selected wall-normal positions in the logarithmic region: (a) $y^{+} = 81.2$, (b) $y_o{}^{+} = 81.2$, (c) $y^{+} = 103.6$, and (d) $y_o{}^{+} = 103.6$. The contour levels are equally spaced from 0.3 to 0.9 with increments of 0.1. The length of the major axis is plotted as a function of the length of the minor axis for (e) $u'^{+}(y^{+})$ and (f) $\Delta u_W'^{+}(y_o{}^{+})$ at four selected wall-normal positions with two Reynolds numbers.

channel flow data with $\mathrm{Re}_\tau = 547$ are simulated. The simulation is conducted in a computational domain of $8\pi h \times 4\pi h \times 2h$ with $N_x = 1536$, $N_z = 1536$, and $N_y = 257$ in the streamwise, spanwise, and wall-normal directions, respectively. The corresponding streamwise and spanwise grid resolutions in viscous units are given by $\Delta x^+ = 13.4$ and $\Delta z^+ = 6.8$, respectively. For the space-time correlation study, 499 raw snapshots with a constant time interval of 0.02 are deployed. The computational code and configurations deployed in this study are validated by the comparisons of the mean and rms profiles with the open-source DNS database [25], as shown in Appendix A.

Figures 13(a), 13(c) and 13(b), 13(d) display the space-time correlation contours as a function of space separation and time delay for the streamwise velocity fluctuation $u'^+(y^+)$ and $\Delta u'^+_W({y_o}^+)$ at two selected wall-normal positions in the logarithmic region, respectively. The corresponding length of the major axis as a function of the length of the minor axis for the contours is plotted in Figs. 13(e) and 13(f) and the results for the channel flow data with $\mathrm{Re}_\tau = 934$ are also included to facilitate comparison. Other wall-normal positions in the logarithmic region have similar characteristics and are not shown here for brevity. It can be seen that the space-time correlations of streamwise velocity fluctuations carried by attached eddies at a given length scale feature wider elliptical shapes and much smaller aspect ratios than those of the ensembled space-time correlations, which is consistent with the results for the channel flow data with $\mathrm{Re}_\tau = 934$. Furthermore, it is not difficult to observe that the aspect ratios for the space-time correlation contours of streamwise velocity fluctuations carried by attached eddies at a given length scale are mainly dominated by the wall-normal position ${y_o}^+$, i.e., the characteristic length scale of attached eddies, rather than the Reynolds number. These visible results are consistent with our previous analyses.

---

[1] A. J. Smits, B. J. McKeon, and I. Marusic, High–Reynolds number wall turbulence, Annu. Rev. Fluid Mech. **43**, 353 (2011).

[2] J. Jiménez, Near-wall turbulence, Phys. Fluids **25**, 101302 (2013).

[3] G. He, G. Jin, and Y. Yang, Space-time correlations and dynamic coupling in turbulent flows, Annu. Rev. Fluid Mech. **49**, 51 (2017).

[4] G.-W. He, M. Wang, and S. K. Lele, On the computation of space-time correlations by large-eddy simulation, Phys. Fluids **16**, 3859 (2004).

[5] L. Guo, D. Li, X. Zhang, and G.-W. He, LES prediction of space-time correlations in turbulent shear flows, Acta Mech. Sin. **28**, 993 (2012).

[6] L. Fu, M. Karp, S. T. Bose, P. Moin, and J. Urzay, Shock-induced heating and transition to turbulence in a hypersonic boundary layer, J. Fluid Mech. **909**, A8 (2021).

[7] L. Fu, S. Bose, and P. Moin, Prediction of aerothermal characteristics of a generic hypersonic inlet flow, Theor. Comput. Fluid Dyn. **36**, 345 (2022).

[8] C. Cheng, X. Chen, W. Zhu, W. Shyy, and L. Fu, Progress in physical modeling of compressible wall-bounded turbulent flows, Acta Mech. Sin. **40**, 323663 (2024).

[9] M. Wang, J. B. Freund, and S. K. Lele, Computational prediction of flow-generated sound, Annu. Rev. Fluid Mech. **38**, 483 (2006).

[10] G. I. Taylor, The spectrum of turbulence, Proc. R. Soc. Lond. A **164**, 476 (1938).

[11] J. C. Del Alamo and J. Jiménez, Estimation of turbulent convection velocities and corrections to Taylor's approximation, J. Fluid Mech. **640**, 5 (2009).

[12] R. de Kat and B. Ganapathisubramani, Frequency–wavenumber mapping in turbulent shear flows, J. Fluid Mech. **783**, 166 (2015).

[13] G. Heskestad, A generalized Taylor hypothesis with application for high Reynolds number turbulent shear flows, J. Appl. Mech. **32**, 735 (1965).

[14] J. Kim and F. Hussain, Propagation velocity of perturbations in turbulent channel flow, Phys. Fluids **5**, 695 (1993).

[15] X. Yang and M. F. Howland, Implication of Taylor's hypothesis on measuring flow modulation, J. Fluid Mech. **836**, 222 (2018).
[16] G.-W. He and J.-B. Zhang, Elliptic model for space-time correlations in turbulent shear flows, Phys. Rev. E **73**, 055303 (2006).
[17] X. Zhao and G.-W. He, Space-time correlations of fluctuating velocities in turbulent shear flows, Phys. Rev. E **79**, 046316 (2009).
[18] R. H. Kraichnan, Kolmogorov's hypotheses and Eulerian turbulence theory, Phys. Fluids **7**, 1723 (1964).
[19] Q. Zhou, C.-M. Li, Z.-M. Lu, and Y.-L. Liu, Experimental investigation of longitudinal space–time correlations of the velocity field in turbulent Rayleigh–Bénard convection, J. Fluid Mech. **683**, 94 (2011).
[20] J. Hogg and G. Ahlers, Reynolds-number measurements for low-Prandtl-number turbulent convection of large-aspect-ratio samples, J. Fluid Mech. **725**, 664 (2013).
[21] W. Wang, X.-L. Guan, and N. Jiang, TRPIV investigation of space-time correlation in turbulent flows over flat and wavy walls, Acta Mech. Sin. **30**, 468 (2014).
[22] S. J. Kline, W. C. Reynolds, F. Schraub, and P. Runstadler, The structure of turbulent boundary layers, J. Fluid Mech. **30**, 741 (1967).
[23] W. Schoppa and F. Hussain, Coherent structure generation in near-wall turbulence, J. Fluid Mech. **453**, 57 (2002).
[24] K. C. Kim and R. J. Adrian, Very large-scale motion in the outer layer, Phys. Fluids **11**, 417 (1999).
[25] J. C. Del Alamo and J. Jiménez, Spectra of the very large anisotropic scales in turbulent channels, Phys. Fluids **15**, L41 (2003).
[26] J. Ahn, J. H. Lee, J. Lee, J.-h. Kang, and H. J. Sung, Direct numerical simulation of a 30R long turbulent pipe flow at $Re_\tau = 3008$, Phys. Fluids **27**, 065110 (2015).
[27] A. Townsend, *The Structure of Turbulent Shear Flow* (Cambridge University Press, Cambridge, 1976).
[28] A. Perry and M. Chong, On the mechanism of wall turbulence, J. Fluid Mech. **119**, 173 (1982).
[29] A. Lozano-Durán, O. Flores, and J. Jiménez, The three-dimensional structure of momentum transfer in turbulent channels, J. Fluid Mech. **694**, 100 (2012).
[30] Y. Hwang, Statistical structure of self-sustaining attached eddies in turbulent channel flow, J. Fluid Mech. **767**, 254 (2015).
[31] A. Lozano-Durán and H. J. Bae, Characteristic scales of Townsend's wall-attached eddies, J. Fluid Mech. **868**, 698 (2019).
[32] C. Cheng and L. Fu, Consistency between the attached-eddy model and the inner–outer interaction model: A study of streamwise wall-shear stress fluctuations in a turbulent channel flow, J. Fluid Mech. **942**, R9 (2022).
[33] C. Cheng and L. Fu, Linear-model-based study of the coupling between velocity and temperature fields in compressible turbulent channel flows, J. Fluid Mech. **964**, A15 (2023).
[34] I. Marusic and J. P. Monty, Attached eddy model of wall turbulence, Annu. Rev. Fluid Mech. **51**, 49 (2019).
[35] M. Guala, S. Hommema, and R. Adrian, Large-scale and very-large-scale motions in turbulent pipe flow, J. Fluid Mech. **554**, 521 (2006).
[36] I. Marusic, W. J. Baars, and N. Hutchins, Scaling of the streamwise turbulence intensity in the context of inner-outer interactions in wall turbulence, Phys. Rev. Fluids **2**, 100502 (2017).
[37] H. Abe, H. Kawamura, and H. Choi, Very large-scale structures and their effects on the wall shear-stress fluctuations in a turbulent channel flow up to $Re_\tau = 640$, J. Fluids Eng. **126**, 835 (2004).
[38] S. Hoyas and J. Jiménez, Scaling of the velocity fluctuations in turbulent channels up to $Re_\tau = 2003$, Phys. Fluids **18**, 011702 (2006).
[39] M. Lee and R. D. Moser, Direct numerical simulation of turbulent channel flow up to $Re_\tau = 5200$, J. Fluid Mech. **774**, 395 (2015).
[40] C. Diaz-Daniel, S. Laizet, and J. C. Vassilicos, Wall shear stress fluctuations: Mixed scaling and their effects on velocity fluctuations in a turbulent boundary layer, Phys. Fluids **29**, 055102 (2017).
[41] I. Marusic, R. Mathis, and N. Hutchins, Predictive model for wall-bounded turbulent flow, Science **329**, 193 (2010).

[42] W. J. Baars, N. Hutchins, and I. Marusic, Spectral stochastic estimation of high-Reynolds-number wall-bounded turbulence for a refined inner-outer interaction model, Phys. Rev. Fluids **1**, 054406 (2016).

[43] S. Hoyas and J. Jiménez, Reynolds number effects on the Reynolds-stress budgets in turbulent channels, Phys. Fluids **20**, 101511 (2008).

[44] J. Jimenez and S. Hoyas, Turbulent fluctuations above the buffer layer of wall-bounded flows, J. Fluid Mech. **611**, 215 (2008).

[45] A. Lozano-Durán and J. Jiménez, Effect of the computational domain on direct simulations of turbulent channels up to $Re_\tau = 4200$, Phys. Fluids **26**, 011702 (2014).

[46] J. Jiménez, Coherent structures in wall-bounded turbulence, J. Fluid Mech. **842**, P1 (2018).

[47] X. I. Yang and A. Lozano-Durán, A multifractal model for the momentum transfer process in wall-bounded flows, J. Fluid Mech. **824**, R2 (2017).

[48] B. B. Mandelbrot, Intermittent turbulence in self-similar cascades: Divergence of high moments and dimension of the carrier, J. Fluid Mech. **62**, 331 (1974).

[49] A. J. Smits, M. Hultmark, M. Lee, S. Pirozzoli, and X. Wu, Reynolds stress scaling in the near-wall region of wall-bounded flows, J. Fluid Mech. **926**, A31 (2021).

[50] J. Kim, P. Moin, and R. Moser, Turbulence statistics in fully developed channel flow at low Reynolds number, J. Fluid Mech. **177**, 133 (1987).

[51] Y. Hwang, Near-wall turbulent fluctuations in the absence of wide outer motions, J. Fluid Mech. **723**, 264 (2013).

[52] G. I. Park and P. Moin, Space-time characteristics of wall-pressure and wall shear-stress fluctuations in wall-modeled large eddy simulation, Phys. Rev. Fluids **1**, 024404 (2016).

[53] H. Choi and P. Moin, On the space-time characteristics of wall-pressure fluctuations, Phys. Fluids **2**, 1450 (1990).

[54] R. J. Adrian, Conditional eddies in isotropic turbulence, Phys. Fluids **22**, 2065 (1979).

[55] C. Cheng, W. Shyy, and L. Fu, Streamwise inclination angle of wall-attached eddies in turbulent channel flows, J. Fluid Mech. **946**, A49 (2022).

[56] A. Perry and I. Marušić, A wall-wake model for the turbulence structure of boundary layers. Part 1. Extension of the attached eddy hypothesis, J. Fluid Mech. **298**, 361 (1995).

[57] R. Deshpande, J. P. Monty, and I. Marusic, Active and inactive components of the streamwise velocity in wall-bounded turbulence, J. Fluid Mech. **914**, A5 (2021).

[58] G. I. Park and P. Moin, Numerical aspects and implementation of a two-layer zonal wall model for LES of compressible turbulent flows on unstructured meshes, J. Comput. Phys. **305**, 589 (2016).

[59] J. Larsson, S. Kawai, J. Bodart, and I. Bermejo-Moreno, Large eddy simulation with modeled wall-stress: Recent progress and future directions, Mech. Eng. Rev. **3**, 15-00418 (2016).